Dalton Transactions

ROYAL SOCIETY OF CHEMISTRY

PAPER

View Article Online
View Journal

Cite this: DOI: 10.1039/c9dt04714j

Electronic influence of substitution on the pyridine ring within NNN pincer-type molecules†

Timothy M. Schwartz, Marianne E. Burnett and Kayla N. Green *

Pincer molecules are of increasing interest due to the modular nature of modification and range of reactivity observed when coordinated to metal ions. A subset within the family of pincer molecules use a pyridine group to bridge the outer two arms as well as provide a N-donor atom for metal binding. While the arm appendages have been studied extensively, little research has been conducted on the electronic effects of the central, substituted pyridine systems. Therefore, a series of NNN pincer-type ligands with substitution on the 4-position of the pyridine ring with –OH, –OBn, –H, –Cl, and –NO_2 functional groups were synthesized and characterized through NMR spectroscopy and ESI-HRMS. Each pincer was metalated with Cu(II) salts and evaluated through X-ray diffraction analysis, cyclic voltammetry, and density functional theory analysis. The results indicate that the relatively unstudied –OBn group demonstrates both electron-withdrawing (XRD bond lengths) and electron-donating (NMR spectroscopy) properties. The –NO_2 pincer ligand shows a redox event within experimental windows evaluated, in contrast to the other congeners studied. In addition, electron-donating groups increase the electron density around the Cu(II) center based on DFT studies and cyclic voltammetry. These findings can be applied to other pyridine-based pincer systems when considering ligand design and warrants future characterization of 4-position substituted pyridines.

Received 11th December 2019,
Accepted 28th January 2020

DOI: 10.1039/c9dt04714j

rsc.li/dalton

Introduction

Pincer molecules have been of extreme interest in the field of organometallic chemistry, amongst others, due to the attractive properties of these ligands. Pincers are loosely defined as terdentate ligands (three coordinating sites), with homo- or hetero-atom sites that prefer a meridional geometry upon metal coordination.[1] van Koten described pincer systems in the late 80s and observed that the terdentate ligand system was highly rigid, easily tunable, and had activity involved in C–H bond activation when bound with a variety of metal-ions including Pt, Pd, Ni, Cu, and Ir.[2] While the ligand system was simple in nature, the pincer metal complexes showed stability and incredible versatility within organometallic chemistry.

Pincers are known for providing outer sphere effects, which are key in organometallic and biological applications.[1,3,4] In coordination chemistry, pincers have continued to be investigated as the inherent features can be easily modified. Specifically, pincer ligands have been manipulated to focus on overall tunability including electronic effects and ring size within the inner coordination sphere. For example, the central atom coordinating to the metal center has *trans* influence on species that may coordinate to the remaining open site of the metal center.[1,5]

Structural modification studies to date have largely focused on modification to the side arm appendages. Fig. 1 shows examples of the diversity in symmetric chiral and achiral arms containing S, P, C, and N hetero-donor atoms.[6–13] The broad selection of these arms allow for specificity in cases like catalysis. Aromatic rings remain a predominant, central component to pincer molecules, where benzene, pyridine, and pyrrole represent the most prevalent systems. However, few studies have

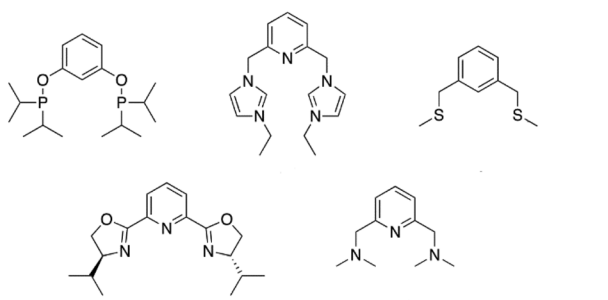

Fig. 1 Notable pincer ligands in the literature.[6–13]

Department of Chemistry and Biochemistry, Texas Christian University, 2950 S. Bowie, Fort Worth, TX 76129, USA. E-mail: kayla.green@tcu.edu

†Electronic supplementary information (ESI) available: NMR spectra, cyclic voltammograms and X-ray diffraction details. CCDC 1958458, 1958460, 1958461, 1958462, 1958464 and 1958465. For ESI and crystallographic data in CIF or other electronic format see DOI: 10.1039/c9dt04714j

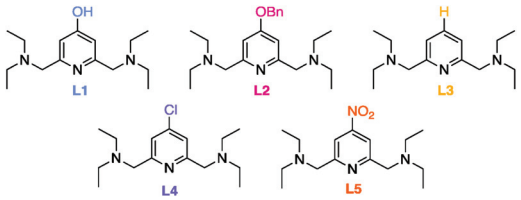

Fig. 2 NNN type pincers described in this report.

focused on functional changes of these aromatic systems within a pincer unit.[14–17] These studies focused mainly on benzene derivatives. Most notably, and specific to this report, functional modifications to pyridine rings are difficult due to the uneven distribution of electron density around the ring. In order to expand the number of NNN type pincers and provide insight into the fundamental properties of these pyridine-derived systems, a new library of pincer ligands was produced. The subsequent studies were used to assess how the electronic modifications affect the coordination chemistry of chelated metal centers.

Herein, we present the synthetic routes to the 4-substituted (–OH (**L1**), –OBn (**L2**), –Cl (**L4**), –NO_2 (**L5**)) congeners of the symmetric NNN pincer 2,6-bis(diethylaminomethyl)pyridine (**L3**) reported previously (Fig. 2).[13] These molecules were characterized through ^{1}H and ^{13}C NMR, and ESI-HRMS. The Cu(II) complex of each pincer was isolated and studied through X-ray diffraction analysis and cyclic voltammetry to evaluate the impact of the substitution on the Cu(II) center. DFT analysis was used to further understand the observations derived from the characterization methods of both the ligands and Cu (II) complexes.

Results and discussion

In order to evaluate the influence of substitution in the 4-position of the pyridine ring with NNN pincer-type ligands, symmetric systems **L1** (–OH), **L2** (–OBn), **L3** (–H), **L4** (–Cl), and **L5** (–NO_2) were produced according to the synthetic routes described in Scheme 1. **L3** has been previously reported by Vedernikov and co-workers using 2,6-bis(tosyloxymethyl)pyridine and diethyl amine.[13] However, a streamlined, new synthetic approach was used and described herein (Scheme 1). The syntheses of **L2–L5** rely on a dialkylhalide precursor, which is subjected to nucleophilic substitution with Et_2NH to produce the ligands of interest. This process was facilitated by the use of excess Et_2NH and K_2CO_3 in CH_3CN with yields

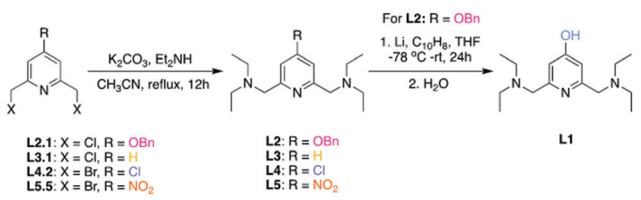

Scheme 1 Synthetic methods used for ligands **L1–L5**.

>87%. Lower yields were obtained in DMF with equimolar amounts of Et_2NH and K_2CO_3 (50–60%). While higher temperatures (85 °C) were used for **L2–L3**, ligands with electron withdrawing groups required lower temperatures (<60 °C) in order to avoid nucleophilic aromatic substitution. **L1** was obtained through the removal of the benzyl group of **L2** using a naphthalene-catalyzed lithiation step from lithium pellets in anhydrous THF at −78 °C followed by hydrolysis with H_2O.[18,19] Care was taken to avoid an increase in temperature during the reaction, which was observed to result in de-aromatization of the pyridine ring. Hydrogenation with palladium catalysts were also not successful. The **L1–L5** pincers were isolated as yellow, transparent viscous oils in the free base form. **L1–L5** are readily soluble in organic solvents. While **L3** is readily soluble in water, **L1–L2** and **L4–L5** require acidification to produce aqueous solutions. These molecules were also observed to be highly hygroscopic and were, therefore, stored under nitrogen. The **L1–L5** ligands were characterized by ^{1}H and ^{13}C NMR, as well as ESI-HRMS (Fig. S1–S15†). Ligands containing electron withdrawing groups (**L4–L5**) have aromatic resonances shifted further downfield, compared to **L3** (neutral) and **L1–L2** (electron donating). It is interesting to note that **L1** has the potential to tautomerize between the keto and enol form (Scheme 2).[20] Based on ^{1}H and ^{13}C NMR, the keto form is the observed tautomer in solution (Fig. S1 and S2†).

Traditionally, Hammett parameters are used to identify the correlation between electron donor ability and an observed result.[21,22] While Hammett parameters are available for –OH, –H, –Cl, and –NO_2, data for –OBn has not been reported in the literature. Such analysis is also challenging because of the keto–enol tautimerization observed with **L1**. Therefore, density functional theory (DFT) was used to understand the trends observed in the NMR spectra. The keto form of **L1** was observed to be more thermodynamically stable (Δ59.9 kJ mol^{-1}). Therefore, only this tautomer will be discussed for the ligand DFT comparisons in Fig. 3. The frontier molecular orbi-

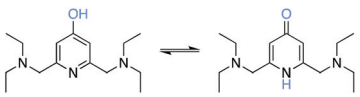

Scheme 2 Keto–enol tautomerization of **L1**.

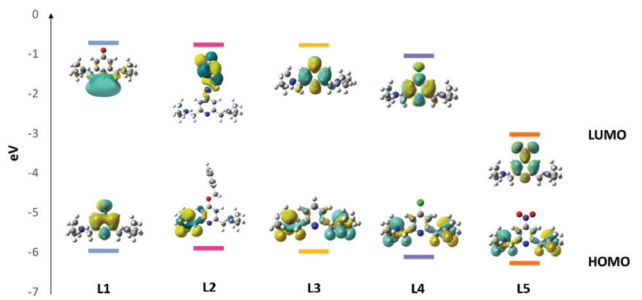

Fig. 3 Relative HOMO–LUMO gaps of ligands **L1–L5** with the respective frontier molecular orbitals.

tals of **L1–L5** show a correlation between the relative HOMO–LUMO gaps and substitution at the 4-position of the pyridine ring. **L1** (5.23 eV) and **L3** (5.20 eV) have larger HOMO–LUMO gaps compared to **L2** (5.12 eV), **L4** (5.08), and **L5** (3.23 eV). These results suggest that the –OBn substituent is more closely related to the electron withdrawing moieties than electron donating moieties. In particular, the noticeably smaller HOMO–LUMO gap of **L5** suggests that ligand-based redox activity could be accessible.

X-ray diffraction analysis

Given these observations, the substitution on the 4-position of the pyridine ring suggested differences in electron donor ability of these pincer ligands. Therefore, we synthesized Cu(II) complexes (Scheme 3) in order to explore these implications to coordination chemistry. Cu(II) salts were chosen because of the straightforward synthetic procedures required, high formation constants predicted by the Irving-Williams series, and relative ease of crystallization within the series.[23] The Cu(II) congener of **L3** has been previously reported in the solid state as [Cu**L3**Cl_2] and was used for comparison herein.[13] Likewise, crystalline materials suitable for XRD analysis were obtained for the Cu(II) complexes of **L1**, **L2**, **L4**, and **L5** using $CuCl_2$ in DCM (Scheme 3a and Fig. 4, 5). Pentacoordinate Cu(II) complexes were isolated with one pincer and two chloro ligands ([Cu**L1**Cl_2], [Cu**L2**Cl_2], [Cu**L4**Cl_2]), and a tetracoordinate Cu(II) complex was isolated with one bound chloro ligand and a noncoordinating $[CuCl_4]^{2-}$ counterion ([Cu**L5**Cl]$_2$[$CuCl_4$]) (Fig. 4 and 5).

In addition, BF_4 salts were hypothesized to facilitate crystallization as non-coordinating counter ions. Therefore, each ligand (**L1–L5**) was dissolved in acidic water (pH ∼ 5), followed by the slow addition of aqueous $Cu(BF_4)_2$ to produce the Cu(II) complexes (Scheme 3b). X-ray quality crystals were obtained for the Cu(II) complexes of **L4–L5** by the vapor diffusion of Et_2O into an CH_3CN solution of the complexes at room temperature and subjected to XRD analysis. The results (Table 2 and Fig. 4, 5) indicate a coordination number of four to the Cu

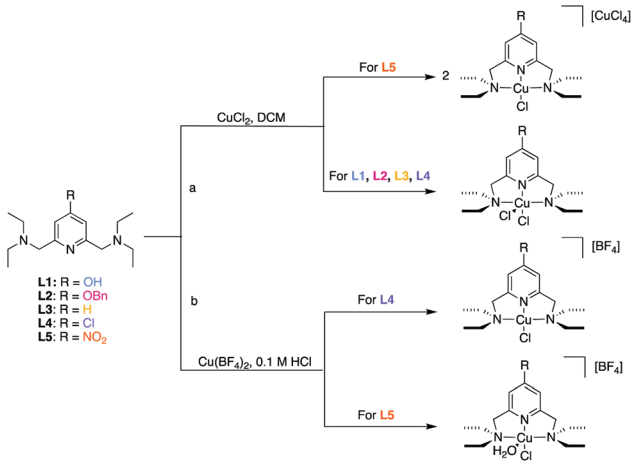

Scheme 3 General metalation procedures using (a) $CuCl_2$ or (b) $Cu(BF_4)_2$.

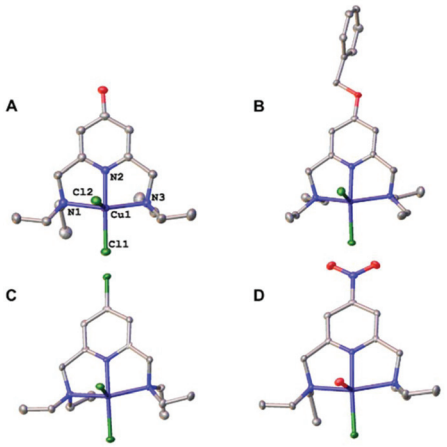

Fig. 4 Solid state structures of pentacoordinate (A) [Cu**L1**Cl_2], (B) [Cu**L2**$Cl_2]_a$, (C) [Cu**L4**$Cl_2]_b$, and (D) [Cu**L5**(OH_2)Cl][BF_4] demonstrating square pyramidal geometry. Counter ion and hydrogen atoms have been removed for clarity.

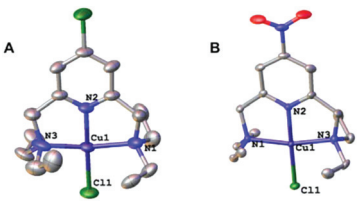

Fig. 5 Solid state structures of tetracoordinate (A) [Cu**L4**Cl][BF_4] and (B) [Cu**L5**Cl]$_2$[$CuCl_4$] with square planar geometry. Counterions and hydrogen atoms have been removed for clarity.

(II) center comprised of one pincer (NNN donors) and one coordinated chloro ligand ([Cu**L4**Cl][BF_4]) and a coordination number of five consisting of one chloro and one aqua ligand ([Cu**L5**(OH_2)Cl][BF_4]) (Fig. 4 and 5). Repeated attempts to obtain crystalline materials of the Cu(II) complexes of **L1–L3** with $[BF_4]^-$ counter ions were unsuccessful.

Each of the pentacoordinate Cu(II) complexes [Cu**L1**Cl_2], [Cu**L2**Cl_2], [Cu**L3**Cl_2], [Cu**L4**Cl_2], and [Cu**L5**(OH_2)Cl][BF_4] are observed in a distorted square pyramidal geometry. The *N*-pyridine-Cu(II) bond lengths vary depending on the moiety on the 4-position of the ring (Table 1). In general, the more electron withdrawing groups have longer bond lengths than the hydrogen congener **L3**, while the electron donating groups have shorter bond lengths. It should be noted that while [Cu**L1**Cl_2], [Cu**L2**Cl_2], and [Cu**L4**Cl_2] were isolated with two chloride ligands coordinated to the Cu(II), the solid state structure of [Cu**L5**(OH_2)Cl][BF_4] has one chloride ligand and one aqua ligand. Attempts to isolate the pentacoordinate $CuCl_2$ salts of **L5** proved unsuccessful, and therefore suggest this is an artifact of the ligand donor ability. Metalation of **L5** with $CuCl_2$ produced the tetracoordinate complex with a $[CuCl_4]^{2-}$ counterion (Scheme 3a and Fig. 5). The incomplete metalation was observed for the isopropyl congener of **L3** previously.[13] We

Table 1 Selected bond lengths (Å) and angles (°) for [Cu**L1**Cl_2], [Cu**L2**Cl_2]$_a$, [Cu**L3**Cl_2], [Cu**L4**Cl_2]$_b$, and [Cu**L5**(OH_2)Cl][BF_4]

	[Cu**L1**Cl_2]	[Cu**L2**Cl_2]$_a$	[Cu**L3**Cl_2]*	[Cu**L4**Cl_2]$_b$	[Cu**L5**Cl(OH_2)][BF_4]
N1–Cu	2.174(3)	2.156(2)	2.122(3)	2.155(5)	2.128(3)
N2–Cu	1.926(2)	1.9473(19)	1.939(2)	1.949(5)	1.945(2)
N3–Cu	2.118(2)	2.184(2)	2.170(3)	2.159(5)	2.126(3)
N1–Cu–N3	153.43(10)	140.95(8)	152.99(9)	152.74(18)	157.37(7)
N2–Cu–Cl	170.98(8)	160.65(6)	167.10(8)	163.60(14)	170.68(5)

* Ref. 13.

Table 2 Selected bond lengths (Å) and angles (°) for four coordinate [Cu**L4**CuCl][BF_4] and [Cu**L5**Cl]$_2$[$CuCl_4$]

	[Cu**L4**Cl][BF_4]	[Cu**L5**Cl]$_2$[$CuCl_4$]
N1–Cu	2.155(9)	2.067(3)
N2–Cu	1.908(3)	1.920(3)
N3–Cu	2.037(10)	2.092(3)
N1–Cu–N3	159.6(3)	166.27(12)
N2–Cu–Cl	178.5(13)	178.96(10)

attribute this observation to the electron withdrawing moiety of **L5**. The electron withdrawing nature of the NO_2 group decreases electron density away on the *N*-pyridine atom and subsequently decreases the donor capability of this ligand making metalation more challenging. While the ethyl arms of [Cu**L4**Cl]BF_4 were highly disordered, those of [Cu**L1**Cl_2], [Cu**L2**Cl_2], [Cu**L3**Cl_2], [Cu**L4**Cl_2], and [Cu**L5**(OH_2)Cl][BF4] were not. For the pentacoordinate complexes, the fifth bound ligand forces the ethyl arms away from the coordination sphere of the Cu(II) center and may be the origin of larger error observed with the four coordinate complexes. It should be noted that refinement of data from the [Cu**L4**Cl_2] material required modeling with twin laws and resulted in lower resolution data compared to other systems described herein.

The experimental bond lengths for the tetracoordinate Cu(II) complex of **L4** are shorter than that of **L5**. However, the pentacoordinate Cu(II) complex of **L4** has the longest bond (1.949(5) Å). This highlights the competitive behavior of this moiety. While the chloro-substituent is electron-withdrawing by induction, it is electron-donating by resonance. Consequently, resonance overshadows the effect of induction, leading to the electron-donating characteristics seen for the [Cu**L4**Cl_2] complex.

Computational analysis

Density functional theory (DFT) analysis was further used to help interpret the experimental observations. As observed with the solid state structure of the Cu(II) complexes, multiple forms of coordination are accessible. Therefore and for simplicity, only the free ligands and the tetracoordinated Cu(II) complexes were modeled. The computations only accounted for ligands coordinated to the metal center and subsequently were modeled as a divalent species with one anionic ligand (chloro ligand) for a total charge of +1. In order to further differentiate computational and experimental complexes, the computed Cu

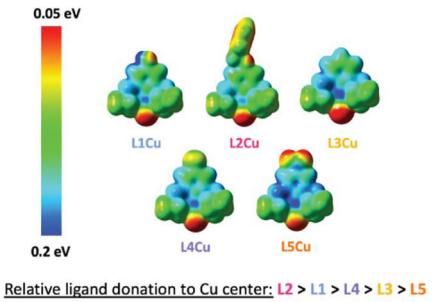

Fig. 6 Electrostatic potential maps of four coordinate Cu(II) complexes with one bound chloro ligand.

(II) complexes are denoted as follows: **L1**Cu, **L2**Cu, **L3**Cu, **L4**Cu, and **L5**Cu. Each structure was optimized using B3LYP 6-31++g(d,p) level of theory. Similar results were obtained using the higher theory 6-311++g(d,p) for **L1**Cu and **L3**Cu, so the former level of theory was used in order to conserve computational resources. Frequency calculations were performed for each structure to verify a lack of imaginary frequencies. Using the computed optimized geometries, energy profiles were modeled for the free ligands and Cu(II) complexes in the form of HOMO–LUMO and SOMO–LUMO diagrams, as well as electrostatic potential maps (Fig. 3, 6 and 7). The majority of the electron density (red) is localized around the chloro-counterion within each complex, as expected. In addition, a deficiency of electron density (blue) is centered around the Cu

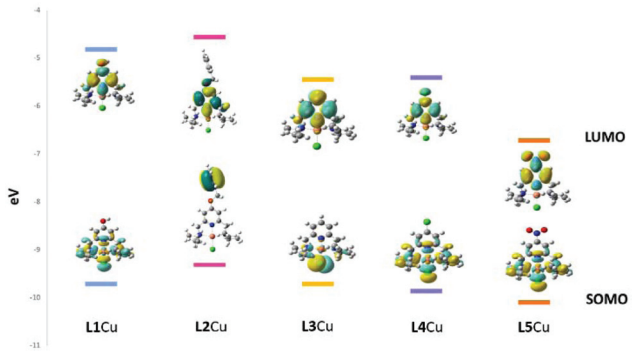

Fig. 7 Relative SOMO–LUMO gaps of **L1**Cu–**L5**Cu complexes, arranged from left to right, with the respective frontier molecular orbitals.

(II) center for each complex (Fig. 6). Interestingly, **L2**Cu shows the greatest electron density around the Cu(II) center. We attribute this observation to the electron-donating ability of the oxygen atom. In contrast, **L5**Cu shows electron density localization around the NO_2-substituent. The electron withdrawing group pulls electron density away from the Cu(II) center. Interestingly, an unoccupied orbital situated around the nitro group 1.8389 eV lower than the HOMO, was observed in Natural Bond Orbital analysis. **L3**Cu and **L4**Cu show almost identical qualitative results. This observation demonstrates the competitive behavior of induction and resonance and is supported by the electrochemistry experiments discussed below.

The fragment orbital contributions to the HOMO, SOMO, and LUMO of the ligands and Cu(II) complexes were also examined with the computer program, Chemissian[24] (Fig. S35–S38†). **L5**Cu again shows the majority of orbital contribution originates from the nitro-substituent. Interestingly, the OBn group within **L2**Cu shows similar results for the SOMO. This raises an interesting question regarding the electronic nature of the OBn substituent as a whole. As expected, **L1** shows HOMO and LUMO contributions from mainly the *N*-pyridine and substitution at the 4-position. This supports the observations of the electron donating properties of this ligand, even in the keto form. Furthermore, the NBO partial charge density on the *N*-pyridine atom were determined (Table S24†). A Hammett plot (Fig. S39†) was constructed for each species, except **L2Cu** because no such parameter exists for the OBn substituent. It is evident that a relationship exists for the partial charge density and the given Hammett parameter values.

Electrochemistry

Cyclic voltammetry studies of the Cu(II) complexes, prepared *in situ*, were carried out in acetonitrile using 0.1 M TBAP, a platinum wire auxiliary electrode, glassy carbon working electrode, and Ag wire reference electrode. The scan rates were varied from 20 mV s^{-1} to 500 mV s^{-1} and referenced to Fc^+/Fc (Fig. 8, S16, S18, S20 and S22†). Notably, the E_{pc} of [Cu**L2**Cl_2] (−594 mV), [Cu**L3**Cl_2] (−592 mV), and [Cu**L4**Cl_2] (−593 mV) measured at 100 mV s^{-1} and assigned as Cu(II)/Cu(I), are identical within experimental error. This supports the computed results found in the ESP maps, which showed similar electronic properties between **L3**Cu and **L4**Cu. The electrochemical behavior of [Cu**L2**Cl_2] and [Cu**L3**Cl_2] are remarkably similar, which contradicts the electron-donating effects modeled in the ESP maps (Fig. 6). We attribute this to the electron-withdrawing capabilities of the benzene ring. No discernable data could be obtained for [Cu**L5**Cl_2]. However, the CV of the **L5** free ligand (Fig. S24†) did show a reversible redox event within the observable window, supporting the results from the small HOMO–LUMO gap seen with the energy computations. The irreversible reduction of [Cu**L1**Cl_2] occurred at a more negative potential (−786 mV) at 100 mV s^{-1}, when compared to the other Cu(II) complexes in the series, and is consistent with the expected electron donating ability of the –OH moiety on the 4-position.

Plots of $v^{1/2}$ *vs.* the I_{pa} and I_{pc} for each Cu(II) complex (Fig. S17, S19, S21 and S23†) show diffusion control up to 100 mV s^{-1} for the oxidation event and up 500 mV s^{-1} for the reduction event (the maximum value evaluated). This observation could be attributed to the inability for the complexes to reorient from the preferred tetrahedral geometry of Cu(I) back to the preferred octahedral geometry of Cu(II), but further studies would be needed to fully understand this phenomenon. The plot of $v^{1/2}$ *vs.* the I_{pa} and I_{pc} for the **L5** free ligand (Fig. S25†) shows diffusion control up to 500 mV s^{-1} (the maximum value evaluated) for both the oxidation and reduction event.

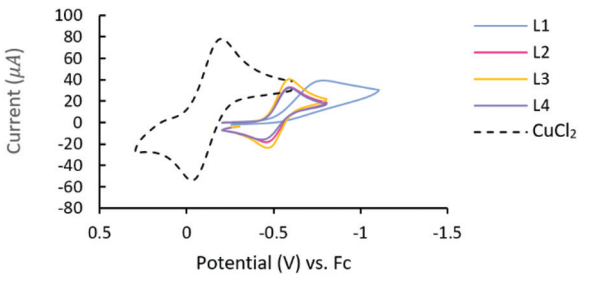

Fig. 8 CV overlay of $CuCl_2$ and the Cu(II) complexes of **L1**–**L4**.

Experimental

Physical methods and general considerations

Caution! Perchlorate salts are explosive and should be handled with care; such compounds should never be heated as solids. Reagents and solvents used for synthesis were purchased from many commercials sources and used as received, unless otherwise noted. All ^{1}H NMR and ^{13}C spectra were completed using a Bruker Avance III (400 MHz) High Performance Digital NMR spectrometer in $CDCl_3$. High resolution mass spectrometry was completed at the University of North Texas Health Science Center by the Advanced Mass Spectrometry and Proteomics Laboratory (Fort Worth, TX). X-ray intensity data were collected on a Bruker D8 Quest diffractometer equipped with a Photon 100 CMOS detector and generator operating at 50 kV and 30 A. The indexing of Bragg intensities was carried out with APEX2 package.[25] Data reduction and absorption corrections were performed with the SAINT[26] and SADABS[27] software packages, respectively. Structures were solved by the direct method using the SHELXL-97 software and refined using SHELXL in the WinGX package. OLEX2 software was used to prepare material and graphics for publication.[28] Cyclic voltammograms were obtained in a nitrogen atmosphere at 22 °C using a BASi EC Epsilon potentiostat equipped with a 3.0 mm glassy carbon working electrode, a platinum wire auxiliary electrode, and quasi Ag wire reference electrode. Measurements were performed with 5 mM samples of each Cu(II) complex in dry acetonitrile with 0.1 M TBAP as supporting electrolyte and Fc as the internal standard ($E_{1/2}$ = 0.00 mV). 4-(Benzyloxy)-2,6-

bis(chloromethyl)pyridine (**L2·1**) was synthesized according to previous work.[29]

4-(Benzyloxy)-2,6-bis(*N*,*N*-diethylaminomethyl)pyridine (L2). **L2·1** (2.0 g, 7.0 mmol), produced using previously reported methods,[29] and K_2CO_3 (2.9 g, 21.2 mmol) were dissolved in 50 mL CH_3CN. Et_2NH (1.5 mL, 14.1 mmol) was added dropwise to the reaction mixture. The reaction was refluxed under N_2 for 12 h. The reaction flask was cooled to room temperature. K_2CO_3 was removed by vacuum filtration. The filtrate was collected and concentrated under reduced pressure. The resulting oil was viscous and dark brown in color (**6**, 2.3 g, 6.7 mmol, 95%). ^{1}H NMR (400 MHz, $CDCl_3$): 7.38 (m, 5H), 7.01 (s, 2H), 5.11 (s, 2H), 3.65 (s, 4H), 2.56 (q, 8H), 1.03 (t, 12H). ^{13}C NMR (100 MHz, $CDCl_3$): 166.00, 161.86, 136.18, 128.61, 128.16, 127.61, 107.08, 69.61, 59.62, 47.34, 11.96. ESI MS (*m*/*z*): Found: 356.26697[**L2** + H]$^+$, theoretical: 356.2624 [**L2** + H]$^+$.

4-(Hydroxy)-2,6-bis(*N*,*N*-diethylaminomethyl)pyridine (L1). Lithium pellets (0.40 g, 57 mmol) and naphthalene (0.90 g, 7.0 mmol) were dissolved in 100 mL of anhydrous THF and sonicated briefly to activate the lithium. The flask was placed under nitrogen over a dry ice-acetone bath. **L2** (1.03 g, 2.89 mmol) was dissolved in a minimal amount of THF and added dropwise to the lithium–naphthalene solution. Upon addition of **L2**, the flask was allowed to come to room temperature but continued stirring under nitrogen for 24 h. After 24 h, water was added to hydrolyze the lithium. The THF–water mixture was washed with diethyl ether (3 × 100 mL). The THF–water layer was collected and concentrated under reduced pressure to produce a light brown solid. The solid was lyophilized. The dry salts were washed with 150 mL absolute ethanol. The ethanol was concentrated under reduced pressure. A light, yellow oil was isolated (**L1**, 0.435 g, 1.68 mmol, 58%). ^{1}H NMR (400 MHz, $CDCl_3$): 6.15 (s, 2H), 3.48 (s, 4H), 2.55 (q, 8H), 2.26 (s, 1H), 1.04 (t, 12H). ^{13}C NMR (100 MHz, $CDCl_3$): 180.79, 147.97, 114.23, 54.22, 47.66, 12.27. ESI MS (*m*/*z*): Found: 266.2206 [**L1** + H]$^+$, theoretical: 266.2154 [**L1** + H]$^+$.

2,6-Bis(*N*,*N*-diethylaminomethyl)pyridine (L3). An optimized method was used that deviated from previously reported studies; spectroscopic characterization were consistent with previous reports.[29,30] Compound **L3·1** (1.00 g, 5.71 mmol) and K_2CO_3 (2.75 g, 19.9 mmol) were added to a flask with approximately 40 mL of acetonitrile. Et_2NH (1.76 mL, 17.4 mmol) was added dropwise to the flask. The reaction mixture was refluxed under N_2 for 12 h. The reaction mixture was cooled to room temperature and subsequently filtered. The filtrate was concentrated under vacuum to yield a light brown oil. The oil was subsequently dissolved in DCM, dried over Na_2SO_4, and concentrated to yield a pale yellow oil (**L2**, 1.24 g, 4.97 mmol, 86.9%). ^{1}H NMR (400 MHz, $CDCl_3$): 7.60 (t, 1H), 7.34 (d, 2H), 3.70 (s, 4H), 2.57 (q, 8H), 1.04 (t, 12H). ^{13}C NMR (100 MHz, $CDCl_3$): 159.77, 136.56, 120.59, 59.68, 47.32, 11.92. ESI MS (*m*/*z*): Found: 250.2254 [**L3** + H]$^+$, theoretical: 250.2205 [**L3** + H]$^+$.

4-Chloro-2,6-lutidine (L4·2). Methods were used based on the literature.[31] 4-Hydroxy-2,6-lutidine (**L4·1**, 8.5 g, 69 mmol) was dissolved in phosphoryl chloride ($POCl_3$, 16 mL, 171 mmol) and heated to 120 °C for 2 h. The reaction was cooled to room temperature before the reaction flask was placed on an ice bath. The $POCl_3$ was quenched with H_2O until effervescence ceased. NaOH pellets were added until a pH of 9. The solution was extracted with dichloromethane (3 × 100 mL). The organic layer was collected, dried over Na_2SO_4, and concentrated under reduced pressure. A light-yellow oil was isolated (**L4·2**, 8.6 g, 60.7 mmol, 91%). ^{1}H NMR (400 MHz, $CDCl_3$): 6.93 (s, 2H), 2.45 (s, 6H).

4-Chloro-2,6-bis(bromomethyl)pyridine (L4·3). A modified procedure from the literature was used.[31] **L4·2** (1.9 g, 13.4 mmol) was placed in a pressure flask and dissolved in 90 mL of carbon tetrachloride. *N*-Bromosuccinimide (NBS, 9.9 g, 55.6 mmol) was added to the flask, which was sealed tightly and heated to 70 °C under a 200 W visible light for 6 h. Upon completion, the reaction was cooled to room temperature. The reaction mixture was filtered through a pad of Celite before being concentrated under vacuum. The resulting dark red oil was collected and dissolved in 140 mL of THF and placed on ice. DIPEA (7.2 mL, 41.3 mmol) was added dropwise to the flask immediately followed by the dropwise addition of diethyl phosphite (8.0 mL, 62.1 mmol). The flask was removed from the ice bath and was stirred at room temperature for 3 h. Water (40 mL) was added to the flask. The reaction mixture was concentrated under reduced pressure until the THF was removed. The resulting aqueous mixture was extracted further using dichloromethane and $NaHCO_3$ solution. The organic layer was collected, dried over Na_2SO_4, and concentrated under vacuum. The resulting oil was purified by column chromatography (10 : 1, hexanes : ethyl acetate). The product (R_f = 0.27) was collected and concentrated under vacuum to afford a light, yellow solid (**L4·3**, 1.6 g, 5.3 mmol, 40%). ^{1}H NMR (400 MHz, $CDCl_3$): 7.39 (s, 2H), 4.48 (s, 4H).

4-Chloro-2,6-bis(*N*,*N*-diethylaminomethyl)pyridine (L4). K_2CO_3 (0.126 g, 1.75 mmol) and **L4·3** (76.1 mg, 0.254 mmol) were added to the reaction flask and dissolved in acetonitrile (10 mL). Et_2NH (0.077 mL, 0.743 mmol) was added dropwise to the reaction mixture, which was stirred at 60 °C for 12 h. The reaction mixture was cooled to room temperature and subsequently filtered. The filtrate was concentrated under vacuum to yield a light orange oil (**L4**, 71.5 mg, 0.252 mmol, 99%). ^{1}H NMR (400 MHz, $CDCl_3$): 7.38 (s, 2H), 3.67 (s, 4H), 2.56 (q, 8H), 1.04 (t, 12H). ^{13}C NMR (100 MHz, $CDCl_3$): 161.91, 145.07, 120.76, 59.28, 47.44, 11.95. ESI MS (*m*/*z*): Found: 284.1863 [**L4** + H]$^+$, theoretical: 284.1815 [**L4** + H]$^+$.

2,6-Lutidine *N*-oxide (L5·2). As reported previously,[31] 2,6-lutidine (**L5·1**) (21.0 mL, 180.3 mmol) was dissolved in glacial acetic acid (56 mL) and H_2O_2 was added dropwise (35.0 mL, 1132.0 mmol). The reaction mixture was heated to 100 °C for 24 h. The flask was cooled to room temperature and concentrated under vacuum. The oil was basified to pH 14 with K_2CO_3 solution and extracted with dichloromethane (3 × 50 mL). The organic layer was collected, dried over Na_2SO_4, and concentrated under vacuum to afford a light-yellow oil (**L5·2**, 24.1 g, 22.2 mmol, 92%). ^{1}H NMR (400 MHz, $CDCl_3$): 6.95 (m, 3H), 2.53 (s, 6H).

4-Nitro-2,6-lutidine *N*-oxide (L5·3). As reported in the previously,[31] compound **L5·2** (9.7 g, 78.8 mmol) was placed in a 100 mL flask. H_2SO_4 (23.0 mL, 422.0 mmol) was added dropwise to the flask. HNO_3 (8.0 mL, 187.8 mmol) was then added dropwise to the flask. The mixture was heated to 85 °C for 24 h and then was cooled to room temperature. The reaction mixture was added dropwise to a flask of water (200 mL) at 0 °C and a white precipitate formed. The aqueous solution was isolated and extracted into chloroform (3 × 100 mL). The organic layer was collected and added to the white precipitate. The organic layer was washed with 1 M NaOH solution (3 × 100 mL). The organic layer was collected, dried over Na_2SO_4, and concentrated under vacuum. A white-yellow solid was isolated (**L5·3**, 9.9 g, 59.1 mmol, 75%). ^{1}H NMR (400 MHz, $CDCl_3$): 8.05 (s, 2H), 2.60 (s, 6H).

4-Nitro-2,6-lutidine (L5·4). As reported in the literature,[31] PCl_3 (8 mL, 92 mmol) was added dropwise to a flask of **L5·3** (5.0 g, 29.7 mmol) dissolved in chloroform at 0 °C. The flask was removed from the ice and heated to 62 °C for 4 h. The reaction was then cooled to room temperature. The reaction mixture was basified to pH 14 with 5 M NaOH. The aqueous mixture was extracted into chloroform and the organic layer was collected, dried over Na_2SO_4, and concentrated under vacuum to afford a light yellow solid (**L5·5**, 3.0 g, 19.9 mmol, 67%) ^{1}H NMR (400 MHz, $CDCl_3$): 7.70 (s, 2H), 2.68 (s, 6H).

4-Nitro-2,6-bis(bromomethyl)pyridine (L5·5). A modified procedure from the literature was used.[31] *N*-Bromosuccinimide (15.7 g, 88.3 mmol) and **L5·4** (2.1 g, 13.8 mmol) were dissolved in benzene (100 mL). The reaction flask was stirred for 3 d at 80 °C under N_2 with irradiation from a 200 W visible light. Solvent was removed under vacuum and the resulting solid was dissolved in diethyl ether (60 mL) and filtered through a Celite and Na_2SO_4 (1 : 1) mixture to remove any un-reacted bromine species. The filtrate was collected and concentrated under vacuum. The red oil was dissolved in anhydrous THF and stirred at 0 °C. DIPEA (9.8 mL, 56.5 mmol) was added dropwise. Next, diethyl phosphite (7.2 mL, 56.5 mmol) was added dropwise. The reaction mixture was stirred at room temperature for 30 minutes. Water was added (100 mL) to quench the diethyl phosphite. The organic volatile solvent was removed under vacuum until the organic layer was removed and the remaining aqueous layer was washed with $NaHCO_3$ and extracted into diethyl ether. The organic layer was collected, filtered through a Celite and Na_2SO_4 mixture (1 : 1), and concentrated under vacuum. The crude product was purified by column chromatography (10 : 1 hexanes : ethyl acetate, R_f = 0.36) to afford a dark red oil (**L5·5**, 1.4 g, 4.2 mmol, 31%). ^{1}H NMR (400 MHz, $CDCl_3$): 8.10 (s, 2H), 4.62 (s, 4H).

4-Nitro-2,6-bis(*N*,*N*-diethylaminomethyl)pyridine (L5). K_2CO_3 (0.12 g, 0.87 mmol) and **L5·5** (0.08 g, 0.25 mmol) were dissolved in 40 mL of acetonitrile in a reaction flask. Et_2NH (0.06 mL, 0.58 mmol) was added dropwise to the reaction mixture, which was then stirred at room temperature for 24 h. The solvent was removed under vacuum. The resulting mixture was dissolved in dichloromethane and washed with water (3 × 50 mL). The organic layer was collected, dried over Na_2SO_4, and concentrated under reduced pressure. The product was isolated as a light orange oil (**L5**, 72 mg, 0.24 mmol, 98%). ^{1}H NMR (400 MHz, $CDCl_3$): 8.09 (s, 2H), 3.80 (s, 4H), 2.61 (q, 8H), 1.06 (t, 12H). ^{13}C NMR (100 MHz, $CDCl_3$): 164.26, 155.49, 113.01, 59.25, 47.62, 12.05. ESI MS (*m*/*z*): Found: 295.21072 [**L5** + H]$^+$, theoretical: 295.2056 [**L5** + H]$^+$.

General method for metalation with $CuCl_2$. A 1.1 : 1 molar ratio of the pincer ligand to $CuCl_2$ was used. The pincer ligand of interest was dissolved in 3 mL of DCM in a small glass vile with a stir bar. $CuCl_2$ was suspended in 3 mL of DCM and added dropwise to the ligand solution with high stirring. The yellow solution instantly changed to an aquamarine color. Upon complete addition of the $CuCl_2$ suspension, a cap was placed on the glass vile and the solution was allowed to stir for 12 h to ensure complete complexation. The solution was passed through a 0.45 μM syringe filter. To the collected DCM was added pentanes to precipitate out the Cu(II) complexes. The light green precipitate was collected and washed with cold pentanes (2 × 5 mL).

General method for metalation with $Cu(BF_4)_2$. A 1.1 : 1 molar ratio of the pincer ligand to $Cu(BF_4)_2$ was used. The pincer ligands were suspended in 2 mL of H_2O in a glass vile with a stir bar and was adjusted to a pH of 5 with 0.1 M HCl. Micelles were still present in the aqueous solution. $Cu(BF_4)_2$ was dissolved in a minimal amount of H_2O and added dropwise to the pincer solution. The yellow solution changed to a deep blue color. A cap was placed on the vile and was set for 12 h with high stirring to ensure complete complexation. The aqueous solution was passed through a 0.45 μM syringe filter. The filtrate was concentrated under reduced pressure to yield a dark blue oil. To this oil was added a minimal amount of CH_3CN and subsequently syringe filtered. The organic filtrate was concentrated under reduced pressure to yield a greenish blue solid.

Conclusions

Overall, four new 2,6-bis(diethylaminomethyl)pyridine derivatives were synthesized by the addition of varied substituents (–OH, –OBn, –Cl, and –NO_2) on the 4-position of the pyridine ring and the synthesis of the –H congener was optimized. The NNN type pincer series were characterized with combinations of ^{1}H and ^{13}C NMR as well as ESI-HRMS. X-ray diffraction analysis and cyclic voltammetry were used to evaluate the Cu(II) complexes. DFT analysis was used to study the electronic effects on both the free ligands and Cu(II) complexes. It was observed that the –NO_2 moiety (**L5**) altered the electronic nature of the free ligand to such an extent that non-innocent redox events were observable in the experimental window of the cyclic voltammetry experiments. NBO analysis showed the presence of an unoccupied orbital lower in energy than the HOMO for both the ligand and Cu(II) complex. Additionally, the –OBn substituent has been relatively unstudied previously. Some experimental methods were indicative of the electron-donating properties (NMR of ligand, DFT) of the oxygen atom,

while others emphasized the electron-withdrawing (XRD of Cu (II) complex) properties of the benzene ring. These observations warrant future studies on the unique properties of this moiety.

Author contributions

The manuscript was written through contributions of all authors. All authors have given approval to the final version of the manuscript.

Conflicts of interest

There are no conflicts to declare.

Acknowledgements

This work was funded by the National Institutes of Health (R15GM123463 (to KG)). The authors are also grateful for generous financial support from TCU Andrews Institute of Mathematics & Science Education (to KG), Cambridge Isotope Laboratories, and TCU Research and Creativity Activity Grant (to KG). The authors acknowledge the TCU High-Performance Computing Center for providing HPC resources. The authors would like to thank Dr. Matthias Zeller from Purdue University for his expertise and structure refinement of [Cu**L4**Cl]BF_4.

References

1 E. Peris and R. H. Crabtree, *Chem. Soc. Rev.*, 2018, **47**, 1959–1968.
2 G. Van Koten, *Pure Appl. Chem.*, 1989, **61**, 1681–1694.
3 D. C. Aluthge, G. Bouhadir, D. Bourissou, B. de Bruin, A. Caballero, M. M. Díaz-Requejo, J. L. Farmer, M. R. Fructos, R. H. Grubbs, P. Gualco, S. T. Liddle, R. J. Lundgren, P. Mehrkhodavandi, D. P. Mills, R. H. Morris, M. Müller, M. G. Organ, K. M. Osten, N. D. Paul, P. R. Payne, P. J. Pérez, A. Pfaltz, M. Pompeo, D. E. Prokopchuk, B. L. Quigley, S. A. Ryken, L. L. Schafer, S. A. M. Smith, M. Stradiotto, J. Urbano, Q. Zhou and S. Zhu, *Ligand Design in Metal Chemistry: Reactivity and Catalysis*, John Wiley & Sons, UK, 2016.
4 R. H. Crabtree, *The organometallic chemistry of the transition metals*, John Wiley & Sons, 5th edn, 2009.
5 J. Choi, A. H. R. MacArthur, M. Brookhart and A. S. Goldman, *Chem. Rev.*, 2011, **111**, 1761–1779.
6 S. Chakraborty, Y. J. Patel, J. A. Krause and H. Guan, *Polyhedron*, 2012, **32**, 30–34.
7 S. Chakraborty, P. Bhattacharya, H. Dai and H. Guan, *Acc. Chem. Res.*, 2015, **48**, 1995–2003.
8 T. Ollevier, *Catalysis*, 2016, **6**, 41–48.
9 G. Bauer and X. L. Hu, *Inorg. Chem. Front.*, 2016, **3**, 741–765.
10 A. M. Tondreau, J. M. Darmon, B. M. Wile, S. K. Floyd, E. Lobkovsky and P. J. Chirik, *Organometallics*, 2009, **28**, 3928–3940.
11 D. Domyati, S. L. Hope, R. Latifi, M. D. Hearns and L. Tahsini, *Inorg. Chem.*, 2016, **55**, 11685–11693.
12 M. Albrecht, P. Dani, M. Lutz, A. L. Spek and G. Van Koten, *J. Am. Chem. Soc.*, 2000, **122**, 11822.
13 A. N. Vedernikov, P. Wu, J. C. Huffman and K. G. Caulton, *Inorg. Chim. Acta*, 2002, **330**, 103–110.
14 J. A. Therrien and M. O. Wolf, *Inorg. Chem.*, 2017, **56**, 1161–1172.
15 G. D. Batema, M. Lutz, A. L. Spek, C. A. van Walree, G. P. M. van Klink and G. van Koten, *Dalton Trans.*, 2014, **43**, 12200–12209.
16 L. A. van de Kuil, H. Luitjes, D. M. Grove, J. W. Zwikker, J. G. M. van der Linden, A. M. Roelofsen, L. W. Jenneskens, W. Drenth and G. van Koten, *Organometallics*, 1994, **13**, 468–477.
17 M. Q. Slagt, G. Rodríguez, M. M. P. Grutters, R. J. M. Klein Gebbink, W. Klopper, L. W. Jenneskens, M. Lutz, A. L. Spek and G. van Koten, *Chem. – Eur. J.*, 2004, **10**, 1331–1344.
18 P. G. M. Wuts and T. W. Greene, *Greene's Protective Groups in Organic Synthesis*, John Wiley & Sons, Inc., Hoboken, NJ, 4th edn, 2007.
19 E. Alonso, D. J. Ramon and M. Yus, *Polyhedron*, 1997, **53**, 14355–14368.
20 K. N. Green, K. Pota, G. Tircsó, R. A. Gogolák, O. Kinsinger, C. Davda, K. Blain, S. M. Brewer, P. Gonzalez, H. M. Johnston and G. Akkaraju, *Dalton Trans.*, 2019, **48**, 12430–12439.
21 L. Hammett, *J. Am. Chem. Soc.*, 1936, **59**, 96–103.
22 C. Hansch, A. Leo and R. W. Taft, *Chem. Rev.*, 1991, **91**, 165–195.
23 H. Irving and R. J. P. Williams, *J. Chem. Soc.*, 1953, 3192–3210, DOI: 10.1039/JR9530003192.
24 S. Leonid, *Chemissian 4.60*, 2005–2018, available at http://www.chemissian.com.
25 Bruker Advanced X-ray Solutions, *APEX2 2007, Version 2014.9-0*, Bruker AXS Inc., Madison, WI.
26 *SAINT*, Bruker AXS Inc., Madison, WI, 2012.
27 Bruker Advanced X-ray Solutions, *SADABS 2001*, Bruker AXS Inc., Madison, WI.
28 O. V. Dolomanov, L. J. Bourhis, R. J. Gildea, J. A. K. Howard and H. Puschmann, *J. Appl. Crystallogr.*, 2009, **42**, 339–341.
29 K. M. Lincoln, P. Gonzalez, T. E. Richardson, L. Rutter, D. A. Julovich, J. W. Simpkins and K. N. Green, *Chem. Commun.*, 2013, **49**, 2712–2714.
30 A. N. Vedernikov, P. Wu, J. C. Huffman and K. G. Caulton, *Inorg. Chim. Acta*, 2002, **330**, 103–110.
31 M. Achmatowicz, L. S. Hegedus and S. David, *J. Org. Chem.*, 2003, **68**, 7661–7666.

